

# Host Galaxies, Obscuration and Nuclear Structure of Three Nearby Compact Symmetric Objects

Eric S. Perlman<sup>1,2,3</sup>, John T. Stocke<sup>4</sup>, John Conway<sup>5</sup>, Chris Reynolds<sup>6,7</sup>

perlman@jca.umbc.edu

## ABSTRACT

We present 3-band HST imaging of three nearby ( $z \leq 0.1$ ) compact symmetric objects (CSOs): 4C 31.04, 1946+708 and 1146+596. These objects were chosen on the basis of proximity to Earth as well as HI 21 cm line absorption. The inner  $H$ -band isophotes of these galaxies are well fit by “nuker” models, typical of nearby ellipticals. Each shows a significant flattening in the isophotal profile at radii  $\sim 0.5''$ , as well as significant variations in ellipticity and PA. However, as previous authors have noted, neither is uncommon for elliptical galaxies. All three objects show modest departures from nuker law models at radii of 1-5  $h_{60}^{-1}$  kpc. Each galaxy shows large, well distributed dust features, which are somewhat concentrated in the nuclear regions in features which resemble disks or tori. We find that the amount of dust in these galaxies is about 10 times higher than normal for ellipticals and radio galaxy hosts. The major axes of the nuclear dust disks tend to be oriented roughly perpendicular to the radio axis. One galaxy, 4C 31.04, exhibits bright nuclear regions well-aligned with the radio axis, while another, 1146+596, shows a significant near-IR excess resembling a stellar bar along its dust disk. The combination of outwardly normal isophotal profiles with significant variations in PA and ellipticity is consistent with the host galaxies being relatively recent merger remnants, with the mergers having occurred  $\gtrsim 10^8$  years ago. Such a merger could have “triggered” the onset of the current active phase seen in these objects, but our data require a significant time delay between the merger event and the onset of nuclear activity. However, these data are also consistent with the hypothesis that the

---

<sup>1</sup>Current Address: Department of Physics, University of Maryland, Baltimore County, 1000 Hilltop Circle, Baltimore, MD 21250.

<sup>2</sup>Department of Physics and Astronomy, Johns Hopkins University, 3400 North Charles Street, Baltimore, MD 21218.

<sup>3</sup>Space Telescope Science Institute, 3700 San Martin Dr., Baltimore, MD 21218.

<sup>4</sup>Center for Astrophysics and Space Astronomy, University of Colorado, Campus Box 389, Boulder, CO 80309-0389.

<sup>5</sup>Onsala Space Observatory, Chalmers Institute of Technology, Onsala, SWE.

<sup>6</sup>Joint Institute for Laboratory Astrophysics, University of Colorado, Campus Box 440, Boulder, CO 80309-0440.

<sup>7</sup>Hubble Fellow

onset of nuclear activity in radio galaxies is due to relatively minor “feeding” events and/or the formation of “bars within bars”, events which would disturb the internal kinematics only slightly.

## 1. Introduction

One of the most enduring mysteries concerning radio galaxies is the trigger for the onset of the active phase. This multifaceted issue strikes at the heart of our understanding of the AGN phenomenon, and yet it is difficult to address because of the high resolutions required to peer into the innermost regions of radio galaxies, and also because of the rarity of the youngest active galaxies.

Observational data now point to the Compact Symmetric Objects (CSOs) and GigaHertz Peaked Spectrum (GPS) radio galaxies as the most likely candidates for being “young” radio galaxies. The distinguishing property of the CSO and GPS classes (heretofore we will use the CSO moniker to refer to both classes; as reviewed by O’Dea 1998, they share most observational properties) is their small lobe separations: typically tens to hundreds of parsecs. Two very recent lines of evidence now point directly to ages  $10^{3-4}$  years, including lobe advance speeds  $\sim 0.1 - 0.3c$  (Owsianik & Conway 1998, Taylor et al. 1998, Owsianik et al. 1998, Conway 2000) and synchrotron aging and energy supply arguments [Readhead et al. 1996a, b; see also Murgia et al. (1999) for similar analyses on CSSs (compact steep spectrum sources) and CSOs]. This “youth” scenario currently appears much more viable than the alternate “frustration” model (e.g., Fanti et al. 1990), which requires an unphysically large amount of material ( $\sim 10^{11}M_{\odot}$ ) within the inner  $\sim 100$  pc (Readhead et al. 1994, DeYoung 1993).

It is natural to ask how (or if) the host galaxies of CSOs differ from those of large-scale, powerful radio galaxies (PRGs). The answer to this question is not yet apparent. On one hand, there should be a continuum of properties, and along these lines recent papers indicate that both CSOs and larger-scale PRGs reside in bright elliptical galaxies with predominantly old stellar populations (De Vries et al. 1998a, 1998b, 2000; Snellen et al. 1996, 1998b; O’Dea et al. 1996). Yet if mergers play a significant role in triggering nuclear activity (see, e.g., Wilson & Colbert 1995), one might expect more dense nuclear interstellar media and unusual nuclear kinematics in the youngest AGN. Along these lines, a few CSOs appear to be highly reddened (O’Dea et al. 1996, De Vries et al. 1998a), their narrow emission line properties argue for higher gas pressures than large-scale PRGs (Fosbury et al. 1987), and 75% of the HI absorption detections among radio galaxies in the unbiased survey of van Gorkom et al. (1989), have turned out to be CSOs (although it may simply be that CSOs are more favorable targets for single-dish HI surveys such as that of van Gorkom et al.; see also Conway 1996).

To date 13 CSOs have been observed with HST. Ten are at  $z > 0.1 - 0.8$  and have been analyzed by McHardy et al. (1994), Perlman et al. (in prep), De Vries et al. (2000), Evans et al.

(1999) and Scoville et al. (2000). Unfortunately, in  $z > 0.2$  objects the limiting resolution of HST is a few hundred to one thousand parsecs, which is insufficient to probe structures comparable to the size of the radio sources in CSOs.

It was with the goal of observing nuclear structure that we observed three CSOs at  $z \leq 0.1$  with HST. These objects were selected because of their proximity to Earth, but also because they had been detected in HI absorption (van Gorkom et al. 1989, Mirabel 1990, Peck, Taylor & Conway 1998). The presence of HI absorption was viewed to be particularly important to test the Wilson & Colbert (1995) hypothesis that the “turn-on” of activity in radio-loud AGN is a product of merger events between possibly active spiral galaxies, because a powerful AGN could blow out dense nuclear gas fairly early in its lifetime via a combination of ram pressure from the radio jet and radiation pressure.

The paper is laid out as follows. In §2 we discuss the observations and data reduction procedures. In §3 we show the images and discuss each galaxy’s morphological and environmental characteristics, including the location of dust lanes and emission features, and relationship to the radio emission. In §4, we discuss the fitting of surface brightness profiles and isophotal models. In §5 we discuss the dust distribution and derive extinction maps. Finally, in §6 we discuss the impact of our results on our knowledge of CSOs and the formation of radio galaxies.

Throughout the paper we assume  $H_0 = 60 h_{60} \text{ km s}^{-1} \text{ Mpc}^{-1}$  and  $q_0 = 0.1$ . Table 1 lists the corresponding physical scale, in parsecs per arcsecond, for each object.

## 2. Observations and Data Reduction Procedures

HST observations were done in three bands, WFPC2 F450W and F702W, and NICMOS F160W (corresponding roughly to  $B$ ,  $R$  and  $H$  bands). The WFPC2 images were taken with the PC1, while the NICMOS images were taken with the NIC1 chip. In Table 1, we give a log of the observations. Due to the high absorbing columns in these sources (plus the typically red colors of both elliptical and spiral galaxies), we chose to integrate significantly longer in F450W than in F702W. The longest integrations were done in F160W, however, because of the HST’s lower sensitivity in the near-IR. The wider field of view of the WFPC2 allowed us to image companion galaxies in the WF chips.

The WFPC2 data were reduced using the best available dark and flat-field images, using the IRAF/STSDAS tasks CALWP2 and CRREJ according to standard recipes. SYNPHOT values in the images headers were used to flux calibrate and transform the images to the standard  $B$  and  $R$  bands.

The NICMOS images were reduced using the best available dark and flat-field images in CALNICA. Since no dithering was done, these images are affected by “grot” and warm pixels. We used UNPEDESTAL (van der Marel 1998) to equalize pedestal levels in the four quadrants of the NIC-

MOS chip; however, we chose not to subtract out the pedestal entirely because of the difficulty of measuring the pedestal when a galaxy occupies most or all of the chip. We resampled the NICMOS image to square pixels (the NICMOS pixels are slightly rectangular), but did not correct for distortion since our main interest in these observations is the central  $\sim 5''$  of each galaxy, for which the corresponding errors in registration are  $\ll 1$  pixel (NICMOS team 1999). The NICMOS images were flux-calibrated and transformed to the standard  $H$  band using the SYNPHOT information in their headers.

Once the images were reduced to this point, we registered the NICMOS and WFPC images. In so doing, we used  $0.0455''$  pixels and assumed the position and orientation of the nucleus on the WFPC images as fiduciary. Two-band ( $B-R$ ) and ( $R-H$ ) color maps were then constructed from the flux-calibrated images (using  $\text{mag}(\text{Vega}) = 0.0$  in each band).

### 3. Host Galaxy Characteristics

In Figures 1-3, we show  $R$ , ( $B-R$ ) and ( $R-H$ ) images. Smaller regions are shown in the color index images than in the F702W image, to bring out detail. Two views of the F702W image are shown in each of Figures 1-3: the top left panel in each figure shows the entire WFPC2 “chevron”, whereas the top right panel shows the inner  $20''$  (for 1146+596) or  $10''$  (for 4C 31.04 and 1946+708).

Below we give a general discussion of the morphological features we find for each object. We also give some background from the literature on each.

**1146+596.** This object (Figure 1) is the nearest of our targets, and is one of the least radio-luminous CSOs. Its milliarcsecond-scale continuum structure is double-lobed, and has been monitored by Taylor, Wrobel & Vermeulen (1998), who detect component advance speeds of  $0.23 \pm 0.05c$ . Unlike most CSOs, 1146+596 has some faint kpc scale radio emission (Wrobel, Jones & Shaffer 1985), which has led some authors (e.g., Conway 1996) to speculate that it might be an example of a recurrent radio source (cf. Reynolds & Begelman 1997). HI observations of this source were made with the VLBA by Peck & Taylor (1998).

The host galaxy is NGC 3894, previously described as an E4 (de Vaucouleurs 1976, 1991), E (Sandage & Tammann 1981) or S0 (Nilson 1973). There is a spiral companion  $\sim 2'$  away (NGC 3895,  $z = 0.0105$ ,  $\sim 25$  kpc projected distance) which is visible on the sky survey plates, and various fainter dwarf galaxies appear on the WFPC2 mosaic (Figure 1a). 1146+596 is the least luminous of the three hosts (Table 2), with an absolute magnitude of approximately  $L^*$ . Ground-based observations found the rare combination of “disky” isophotes (i.e., positive isophotal moment  $a_4$ ), at radii  $\lesssim 5''$ , but “boxy” isophotes (i.e., negative  $a_4$ ) at radii  $\gtrsim 10''$  (Bender, Döbereiner & Möllenhoff 1988; Nieto & Bender 1989; Nieto, Poulain & Davoust 1994). Bender and collaborators also reported an anomalous rotation curve and a M/L ratio about 3 times higher than typical for their sample. The work of Kim (1989) revealed a kiloparsec-scale dust disk, with associated  $H\alpha$  line emission. The source has been detected with IRAS, and from those data Forbes (1991) calculated

a mass of  $1.8 \times 10^7 M_{\odot}$  of cold dust, very large for an elliptical galaxy. The object was first detected in HI absorption by Dickey (1986), and also appears in the sample of van Gorkom et al. (1989).

In our WFPC2 data, the nuclear emission appears rather irregular in shape, due to the presence of two dust lanes. These dust features are very narrow ( $\sim 0.1''$ ), extend  $\sim 300$  pc on either side of the nucleus, and are oriented nearly perpendicular to the arcsecond and milli-arcsecond radio axes (Figures 1c, 1d). The dust lanes are considerably redder than the surrounding galaxy:  $(R-H) \sim 1.3$  mag compared to  $\sim 0.8$  mag, and  $(B-R) \sim 2 - 2.5$  mag compared to  $\sim 1.5$  mag. The observed colors and geometry are consistent with the northwestern and southeastern branches representing (respectively) the foreground and background (with respect to the nucleus) halves of a dust torus at inclination angle  $\sim 70^\circ$ , an interpretation supported by the HI distribution and kinematics (Peck & Taylor 1998). There are also two dusty “loops” on either side of (and connected to) the dust disk, as well as patchy features in the outer parts of the galaxy. When elliptical galaxy isophotes are subtracted from the F160W image, there is a “bar”-like feature in the residuals (Figure 1e) along the dust disk, suggesting either star formation within the region of the dust disk or a non-axisymmetric potential in the nuclear regions (which could drive a radial inflow of gas; Shlosman, Frank & Begelman 1989). This “bar” also appears in the  $(R-H)$  color map. The HI opacity appears to be higher on the northwestern lobe (Peck & Taylor 1998); this is consistent with the redder colors observed in that part of the dust disk.

**4C31.04.** This object (Figure 2) is associated with the galaxy MCG 5-4-18. The HI absorption was first detected in single-dish observations by van Gorkom et al. (1989), and Mirabel (1990) also noticed a high-velocity cloud which later VLBA observations revealed was projected against the galaxy’s center (Conway 1999). The source was detected with IRAS (Impey, Wynn-Williams & Becklin 1990), yielding evidence of considerable dust emission; those authors, however, did not calculate a dust mass. The VLBI radio morphology of the object has been discussed by Conway (1996, 1999), but there is as yet no estimate of lobe advance speeds for this object.

There is a companion galaxy  $20''$  away (MCG 5-4-17,  $z = 0.055$ , 20 kpc projected distance) which is visible on both sky survey plates and our WFPC2 image (Figure 2a), as well as various fainter galaxies which could well form a group associated with the object. Neither the host to 4C31.04 nor its spiral companion shows “tidal tails” or other large-scale evidence of interaction.

The optical galaxy is about two magnitudes brighter than  $L^*$  (Table 2). It is permeated with obscuration features in both the nucleus and outer regions. The nucleus extends perpendicular to the majority of the nuclear dust, with cone-like features very closely aligned with the radio structure. The western extension is somewhat redder [ $(R-H) \approx 1.5$  mag] than the eastern one [ $(R-H) \approx 1$  mag]. By comparison the mean color of the galaxy is  $\langle(R-H)\rangle \approx 1.25 \pm 0.21$  mag. The nuclear obscuration is concentrated in two regions. The first is a very red [ $(R-H) \approx 2$  mag] disk-like feature, oriented close to  $90^\circ$  from the radio axis, which extends  $\sim 500$  pc to the north, and  $\sim 1$  kpc to the south of the nucleus. There are also two 500 pc long “arms” which are less reddened than the disk. These extend both east and west before turning to a more southerly

direction, and connect with the southern part of the disk. A disk of similar size and orientation to the one shown in these images, was predicted by Conway (1999) based on VLBA HI maps. Those maps show that the HI opacity is higher on the Eastern side, but patchy obscuration extends to the West side. A significant amount of patchiness is likely required to reconcile the obscuring features observed in the HI and HST images, although we note that the size scales are rather different. The HI observations were modelled by a disk of atomic gas of radius 500-1000 pc and thickness 100 pc, inclined within  $20^\circ$  of edge-on.

**1946+708.** This object (Figure 3) is our most distant target. It was first detected in HI by Peck, Taylor & Conway (1998; see also Conway 1996). Taylor & Vermeulen (1997) have presented an excellent discussion of multi-year VLBI monitoring of this source, which constrains the angle between the radio jet axis and our line of sight to  $65 - 80^\circ$ . There is a bright companion galaxy about  $1'$  away (67 kpc projected distance, redshift not listed in NED), which is visible on the WFPC image, as well as a number of fainter companions which may form an associated group (although the redshift of these objects is not known).

The host galaxy is about two magnitudes brighter than  $L^*$  (Table 2). The nuclear regions are somewhat redder than the outer regions of the galaxy [ $(B - R) \sim 2 - 3$  mag compared to  $\sim 1.5 - 2$  mag]. This galaxy exhibits nuclear obscuration, which appears to have an inclined, disk-like morphology. The disk is about 600 pc in radius and its major axis could be about  $60^\circ$  from the radio axis.

The HI absorption data for this object are complicated: while the highest HI opacities are observed NE of the nucleus, this is only because that component is very narrow in velocity space. Much higher column densities, in fact, are seen against the core and SW of the nucleus (Peck, Taylor & Conway 1999), where the velocity width of the absorption is much higher. Taylor & Vermeulen (1997) and Peck et al. (1998) cite this as evidence that the NE jet is approaching. Free-free absorption has also been detected against the SW jet, suggesting that some of the obscuring material is ionized. Both our HST images and the radio HI data can be explained by an inclined disk, but the pattern of obscuration is not what one would expect because the highest optical obscurations are not seen at the same point as the highest HI columns. The obscuring material is therefore likely to be azimuthally non-uniform, perhaps also with a varying gas to dust ratio.

#### 4. Isophotal Profiles

We fit isophotes for the host galaxies using ELLIPSE and BMODEL in IRAF. In doing so, we excluded obvious isophotal features such as the aligned nuclear emission ‘cones’ observed in 4C31.04 or the bar observed in 1146+596. This process was done iteratively, as some features did not immediately evidence themselves before the initial fitting. In Figure 4, we show the isophotal profile for each galaxy. This figure includes plots of surface brightness, ellipticity, PA, and moments. The isophotes shown in Figure 4 represent the H band data; while isophotes were also extracted

from the R and B band images, the H band data are less affected by dust (cf. §5) and therefore are more representative of the mass distribution of the galaxies.

Figure 4 also shows several other aspects of the isophotal profile: PA and ellipticity as well as isophotal moments. As can be seen, all three objects display significant changes in ellipticity and PA within the range of semi-major axes shown. With the possible exception of the large-scale change in ellipticity in 4C31.04, all of the features seen in these plots can be traced to the images shown in Figures 1-3 (recall, however, that a few obvious features were excluded from the fits). It is likely that some of the largest-ellipticity isophotes extracted in 4C31.04 (i.e., at nuclear distances  $< 0.4''$ ) are a byproduct of flagging the nuclear emission ‘cones’, so we exclude them from further discussion. Note, however, that this cannot explain the larger scale (at radii up to  $\sim 4''$  or 4000 pc) changes in ellipticity observed, as the ‘cones’ extend over less than  $1''$ . Importantly, the amount of variation we see in PA and ellipticity is not unusual for elliptical galaxies, as shown by the data of Bender et al. (1988), who give many examples of objects where (for example) isophotal twists of several tens of degrees, or changes in ellipticity from 0.1 to 0.4, are seen.

The surface brightness profiles of these galaxies cannot be well-fit by generalized models of the form  $I(r) \propto \exp(-\alpha r^\beta)$ . In this formulation,  $\beta = 1$  represents an exponential disk, whereas  $\beta = 0.25$  represents the classical DeVaucouleurs’ profile. All three show essentially power law surface brightness distributions at radii larger than 1 arcsecond, with significant flattenings at small radii (respectively  $\sim 0.7''$  in 1146+596,  $\sim 0.5''$  in 4C31.04 and  $\sim 0.3''$  in 1946+708). This is a common feature among elliptical galaxies, and a signature of ‘nuker’ models (Byun et al. 1996, Faber et al. 1997), which represent the best fits to the nuclear regions of nearby elliptical galaxies at HST resolutions (see also Rest et al. 2001). The nuker models have the mathematical form

$$I(r) = I_b 2^{(\beta-\gamma)/\alpha} \left(\frac{r_b}{r}\right)^\gamma \left[1 + \left(\frac{r}{r_b}\right)^\alpha\right]^{(\gamma-\beta)/\alpha}, \quad (1)$$

where  $r_b$  is the point of maximum curvature in log-log coordinates,  $I_b$  is the surface brightness at  $r_b$ , the asymptotic logarithmic slope inside  $r_b$  is  $-\gamma$ , the asymptotic outer slope is  $-\beta$ , and  $\alpha$  parametrizes the sharpness of the break.

Nuker models were fit to the isophotal profiles using an IDL program that employs the CURVEFIT utility, which uses a generalized, weighted least-squares fitting algorithm. Initial guesses for  $\gamma$ ,  $\beta$ ,  $r_b$  and  $I_b$  were determined using by-eye estimation. Gaussian errors were used to weight the data. We did not extract isophotes at semi-major axes smaller than  $\sim 0.2''$  as this is approximately the FWHM of the HST PSF in H band.

The nuker model fits are overplotted on the surface brightness profiles in Figure 4. As can be seen, the nuker models fit well for all three objects; the best fit parameters are given in Table 2. All three show deviations at large radii: in 4C 31.04, there is a clear excess at radii  $\gtrsim 3.5''$  (3500 pc), in 1946+708 the nuker model overpredicts the observed isophotes at radii  $\gtrsim 1.5''$  (2500 pc), and in 1146+596 we see a slight excess above the nuker models at  $r \gtrsim 4''$  (900 pc).

In Figure 5, we show the  $\alpha, \beta, \gamma, r_b$  values of these objects compared to the sample of Faber et al. (1997). As shown, by this measure the surface brightness profiles of these objects are not visibly abnormal compared to the samples of Faber et al. (1997) and Rest et al. (2001). 1946+708 appears to be what Faber et al. would call a “power-law” galaxy (despite having a significant, if small, break at  $\sim 0.3''$ ), while 4C31.04 and 1146+596 seem to be intermediate between the “core” and “power-law” classes of Faber et al. However, all of these galaxies, and particularly 4C 31.04 and 1946+708, are more distant than any of the objects in the Faber et al. (1997) sample. As noted by Faber et al., in distant galaxies bulge characteristics ‘blend’ with those of the larger galaxy. This would cause the fitted values of  $\gamma$  and  $r_b$  to be larger than they truly are (see their Figures 2 and 3, where Faber et al. simulate the effect of fitting the profiles of M31 and M32, placed at the distance of the Virgo cluster). If their significantly larger distance is accounted for, it is likely that all three are “core” galaxies similar to other bright  $L > L^*$  ellipticals.

The moments of the surface brightness distribution,  $a_3, b_3, a_4, b_4$  (bottom four panels in each column of Figure 4), for these objects all change sharply at very close to the same radii where flattenings in the isophotal profiles are seen (above). In all three objects, we observe the moment  $a_4$  become sharply negative at small radii. The other moments also show significant departures in the inner regions of each galaxy. 1146+596 shows a sharp increase in the moments  $a_3, b_3$ , and  $b_4$  at radii  $\sim 0.7''$ , but at radii  $\sim 0.3''$ ,  $b_3$  and  $b_4$  decrease sharply and become negative. This is consistent with the near-IR bar observed in this object, although the variations at  $0.3'' - 0.7''$  may indicate that some obscuration still remains in the  $H$  band image. By contrast, in 4C31.04, we observe fairly smooth, monotonic decreases in all four moments, beginning at radii  $\sim 0.5''$ . This pattern is indicative of the nuclear emission cones observed in this object. In 1946+708, we observe small increases in  $a_3$  and  $a_4$  at radii  $0.4'' - 0.6''$ , and then decreases in all four moments at radii  $< 0.4''$ . These features are more difficult to trace, because unlike 4C31.04 and 1146+596, there are no obvious features in the H band residuals of this object. However, these changes are somewhat similar in pattern to those observed in 1146+596, and as can be seen in the  $(B - R)$  and  $(R - H)$  color images, 1946+708 exhibits a nuclear dust disk at these radii, as does 1146+596 at radii where sine-wave like variations are seen in the moments. If this interpretation is correct, we might expect that some obscuration remains in these objects at  $H$  band. This interpretation is also consistent with the small changes in ellipticity and PA observed at similar radial distances in 1946+708.

These objects also show some larger scale isophotal features, but as can be seen in Figure 4, the departures in the isophotal moments are much smaller than in the nuclear regions. At  $r > 1''$ , 4C 31.04 appears to have a “disky” profile, consistent with the presence of two larger-scale, spiral shaped dust lanes noted earlier. Diskiness was also previously noted in 1146+596 at radii of  $\sim 2 - 10''$  by Bender et al. (1988); we see this in our data as well, but we are not sensitive to the change to boxy isophotes they noted in this object at radii  $> 10''$ . In both 4C 31.04 and 1146+596, we also see significant departures in the other moments at these larger radii.

The variations that we see in all the isophotal moments at small radii indicate that the kinematics in the inner regions of these objects are likely to be irregular. This is to be expected in



”boxy” (i.e.,  $a_4 < 0$ ) objects; as noted by Nieto & Bender (1989), boxiness tends to be correlated with large kinematic anisotropies. Interestingly, Bender & Nieto (1989) note that boxy isophotes tend to predominate in active elliptical galaxies on kiloparsec scales, thus possibly linking isophotal and kinematical anisotropies to the feeding of AGNs. By contrast, in ”disky” (i.e.,  $a_4 > 0$ ) galaxies, the usual kinematic signature is a rotationally flattened disk, but much less prominent anisotropy (Bender 1988). Thus we can feel secure in saying that by far the most prominent kinematic feature of these objects is likely to be large anisotropies at small radii. We will return to this and related topics in §6.

## 5. Obscuration Features and Distribution

We have used the multi-color HST images to obtain estimates of the total extinction in  $B$  band,  $A_B$  (see Figure 6). In so doing, we made three assumptions. The first assumption is that the average colors of each object are taken as representative of the unextincted stellar population of the host. Since none of these objects appear to be disk-dominated objects seen along their disks, this should be very nearly true if these galaxies follow an extinction law similar to that for our own Galaxy (see Mathis 1990), where by  $H$ -band the extinction is only 6% of what it is in  $B$ -band. We also assume a covering factor of unity, the most conservative assumption, but it is likely that there is some variation in the covering factor, just as in our own Galaxy. Our final assumption is that the overall galaxy colors are dominated by continuum emission, rather than lines. Without emission line imaging we cannot comment on the validity of this assumption. Once these assumptions are made, we can then compute  $A_B$  values for each pixel  $(i, j)$  via

$$(A_B)_{ij} = (B - H)_{ij} - \langle (B - H) \rangle. \quad (2)$$

The nuclear dust disks represent the highest-extinction features seen in each host galaxy. In 1146+596, the northwestern branch of the dust disk reaches  $A_B = 0.9 - 1.1$  mag, while the southeastern branch reaches somewhat lower values ( $A_B = 0.7 - 0.9$  mag). There is considerable extinction as well in between the two visible branches of the central dusty region ( $A_B = 0.5 - 0.7$  mag), suggesting that the nuclear dust torus is filled, rather than open. Somewhat larger extinction values are seen in the disks of 4C31.04 and 1946+708. In 4C 31.04, the disk appears nearly edge-on, with  $A_B = 1.5 - 2.3$  mag, peaking southwest of the galaxy’s nucleus. In 1946+708, which appears to have a somewhat inclined disk, we see  $A_B$  peaking at about 2.0 mag at the northern extremum of the disk, and a much larger variation in extinction, varying between 0.4 and 1.8 magnitudes, with the minimum value of  $A_B$  at the disk’s southwestern edge.

We find lower  $A_B$  values in the dust “loops” of 1146+596 and 4C 31.04, than in their respective nuclear dust disks. In 4C 31.04, the extinction values in the “loops” range from  $A_B = 1.0 - 1.3$  mag in two spots, to the northwest of the nucleus and where the loop intersects with the northern extension of the disk, to values as low as 0.1 – 0.2 mag east and southeast of the nucleus. By

comparison, in 1146+596, the extinction in the “loops” ranges from  $A_B = 0.4 - 0.5$  mag in the loop to the north of the nucleus to only  $0.15 - 0.3$  mag south and east of the nucleus.

1146+596 and 4C 31.04 also exhibit extinction features in their outer regions. In 1146+596, these are patchy, and have moderate  $A_B$  values ( $A_B = 0.3 - 0.7$  mag). In 4C31.04, the large-scale extinction features are distributed in an S-shaped lane, extending outwards from the nuclear disk on both sides for up to 4 kpc. The values of  $A_B$  in this feature range from 0.7–1 mag in the northern lane to 0.2–0.5 mag in the southeastern lane.

The  $A_B$  values can be transformed into HI columns by assuming the extinction law of Mathis (1990), and the  $E(B - V) \rightarrow N(H)$  relationship of Bohlin et al. (1978), viz.  $N_H = 5.8 \times 10^{21} \text{ cm}^{-2} \text{ mag}^{-1}$ . Total dust masses were obtained by integrating the  $N(H)$  maps and a dust-to-gas ratio similar to that of our own Galaxy ( $\sim 100$  by weight). This yields the values given in Table 3. As can be seen, all three of these galaxies have significant HI columns and dust masses typical of spiral galaxies. By comparison, ellipticals typically have dust masses an order of magnitude lower (Goudfrooij et al. 1994a, b), although there are notable exceptions, including some large scale FR II radio sources (de Koff et al. 2000; see also §6). We note in the captions to Figure 6 what the  $A_B$  greyscales of each extinction map corresponds to in terms of  $N_H$ , under the above assumptions.

The  $N_H$  maps allow us to estimate the  $T_s/f_c$  values on each side of the radio source by comparing the values we calculate with  $N_H$  values derived from VLBI observations (Peck & Taylor 1998, Conway 1999, Peck et al. 1999). To do this, of course, one must assume that the same gas serves as the absorbing column for both the radio and optical emission, a nontrivial assumption given that there is a resolution mismatch of approximately a factor 5-10 between the VLBA observation and our HST observations. So these are fairly rough estimates and at most we can differentiate between the two sides of the radio source and not on a point by point basis. Nevertheless, the results are given in Table 3. For all three objects, values of  $T_s/f_c \sim 100 - 200$  K are obtained, even though the dust and gas are within  $\sim 100$  pc of the nucleus. For two objects, 1146+596 and 4C 31.04, our results are roughly consistent with the assumptions of  $\sim 100$  K in the literature (Peck & Taylor 1998, Conway 1999). However, for 1946+708, our results are inconsistent with the assumption by Peck et al. (1998) of  $T_s \sim 8000$  K, unless a very low filling factor is invoked. This is a significant result, even given the resolution mismatch and different methods used in the calculation. To reconcile the two temperature results in a covering factor  $f_c \sim 0.025$ , which we believe is unlikely given the rather uniform appearance of the obscuring screen shown in Figure 6c. As one can see by comparing our Figure 6c to the maps in Peck et al. (1999) the ratio between the thickness of the densest part of the obscuring disk and the the width of the 1.3 GHz continuum emitting region is about 5:1, so that a rather unlikely combination of orientations for the radio minilobes and dust clouds would be required. Further, we note that at  $T = 8000$  K and the densities calculated for this temperature by Peck et al. (1999), one would not expect 21 cm HI absorption due to collisional quenching.

## 6. Discussion

The hosts of these three CSOs appear typical of nearby elliptical galaxies in many respects. All three are ellipticals, well-fit by “nuker” models (Faber et al. 1997) within  $\sim 3$  kpc of the nucleus. All three show significant breaks to flatter cores in their surface brightness distributions, although none actually fall into the “core” region as defined by Faber et al. (1997). Instead, two objects, 1146+596 and 4C31.04, fall into the intermediate region of the  $(r_b, \gamma)$  plane, while 1946+708 falls into the “power-law” section of that diagram. As noted in §4, however, the true values of  $r_b$  and  $\gamma$  for 4C 31.04 and 1946+708 are likely smaller, given their distance and the fact that HST barely resolves the cores in these objects. The hosts of 4C 31.04 and 1946+708 are about 2 magnitudes brighter than  $L^*$ , which is fairly typical of radio galaxy hosts (e.g., Martel et al. 1999, Ledlow & Owen 1995, Smith & Heckman 1989, Owen & Laing 1989), but 1146+596 is somewhat underluminous compared to most radio galaxy hosts, with  $L \approx L^*$ .

As noted in §4, these objects have significantly non-relaxed isophotes at radii of a few hundred parsecs, with significant variations in ellipticity and PA, as well as significant deviations in the isophotal moments. Taken together, this is a fairly sensitive indication that the inner regions of the underlying galaxies are not completely relaxed (e.g., Mihos et al. 1995, Mihos & Hernquist 1996), even if they show no outward indications of a recent merger. Indeed, if the kinematic and morphological properties of elliptical galaxies follow the same relationship on scales of tens to hundreds of parsecs as they do on scales of kiloparsecs, this is a likely indication of large nuclear kinematical anisotropies in these objects. In order to understand the overall impact of this observation, we must assess not only how unusual such variations are, but also assess any resolution related and other biases. Some caution is warranted at the smallest radii (Rest et al. 2001), i.e., at resolutions  $< 0.2''$  HST’s sensitivity to detecting real isophotal twists decreases significantly, such that for a cuspy model with constant ellipticity and PA, ELLIPSE still would erroneously detect some changes in ellipticity and PA on scales smaller than  $0.2''$ . This concern is particularly applicable to 1946+708, which has a large change in ellipticity at  $0.3''$ . Further, we must also exclude from our analysis the isophotes within  $\sim 0.4''$  for 4C 31.04 because they are heavily affected by the masking of the nuclear emission “cones” in that object (cf. §4)

With these caveats in mind, then, we are left with 2 objects (4C31.04 and 1146+596) which have ellipticities that vary between 0.10 and 0.40 in the inner 2-4 kpc, and one (1946+708) which shows much smaller variations. Similarly, 4C31.04 and 1146+596 exhibit major isophotal twists (by several tens of degrees) while 1946+708 exhibits much less variation in PA. Such variations in ellipticity and PA are not at all uncommon in the nearest elliptical galaxies on the 100-1000 pc level (Bender et al. 1988). In 1146+596, we see an ellipticity that decreases fairly steadily in the inner few hundred parsecs. This is consistent with the “diskiness” found on  $2 - 10''$  scales by Bender et al. (1988) in ground-based data. The pattern of the variations seen in 4C31.04 is somewhat reversed; however, this could still be consistent with significant “diskiness” on 500-2000 pc scales (as indicated by the positive values of  $a_4$  we observe at these scales) in a more face-on orientation, and it would be consistent with the larger scale dust lanes in this object noted in §§3 and 5.

These galaxies are somewhat unusual compared to the hosts of most radio galaxies in the amount of nuclear and galaxy wide dust. Martel et al. (1999) analyzed HST WFPC images of 46  $z > 0.1$  3CR radio galaxies, and further analyses of the dust properties of the sample were done by de Koff et al. (2000) and Martel et al. (2000). About half of the 3CR galaxies have some sort of dust feature, including irregular lanes, filaments, nuclear or large-scale disks above a threshold detection level of  $\sim 3 \times 10^4 M_\odot$  in dust. That amount of dust is consistent with the amounts of dust found in non-active elliptical galaxies by Goudfrooij et al. (1994a, b) and Tran et al. (2001). As can be seen, therefore, these objects have dust masses  $0.5 - 1$  dex higher than typical for elliptical galaxies and radio galaxy hosts, although 9/46 3CR hosts are comparable to 1146+596, 4C 31.04 and 1946+708. Interestingly, it is not just the smallest 3CR sources that have substantial dust masses: e.g., 3C 46, 3C 236 (but see below) and 3C 306.1 are all large ( $\gtrsim 1 h_{60}^{-1}$  Mpc) and have  $M_{\text{dust}} > 10^5 M_\odot$ . The 3CR objects with prominent dust lanes also show a significant, but not universal, anti-correlation of dust lane position angle with radio axis, similar to these objects. Somewhat similar results were seen in the HST snapshot survey of BL Lacs undertaken by Urry et al. (2000) and Scarpa et al. (2000). Of the 58 objects in that sample with resolved hosts, 12 were at  $z < 0.1$ , and only one of those (1ES1959+650) has an obvious dust feature: a kpc-scale disk with an estimated dust mass of  $\sim 5 \times 10^5 M_\odot$ , in the same range as these CSOs (Scarpa et al. 2000).

Given the large amount of nuclear dust shown by these observations, it is natural to wonder whether these objects are typical of CSOs in general. While these objects were chosen partly because of their HI absorption, we note that this is a property which is common among CSOs, since up to 50% of CSOs now appear to be HI absorbers (Conway 1996, 2001). Thus, any such bias in this regard is small, although observations of non-HI absorbers might be helpful to elucidate this further.

None of our objects show obvious nuclear point sources, consistent with their strong nuclear obscuration. Martel et al. (1999) found nuclear point sources in 43-54% of  $z < 0.1$  3CR radio galaxies, and some correlation between the lack of a point source and nuclear absorption. Chiaberge, Capetti & Celotti (1999), working with a very similar sample, found a strong correlation between the optical flux of the central compact core and the radio core flux, and an anti-correlation between optical core flux and dust content.

Only one other  $z < 0.2$  CSO has been observed with HST: PKS 1345+12 ( $z = 0.122$ ; Evans et al. 1999, Scoville et al. 2000, Surace et al. 1998). Like our targets, PKS 1345+12 was detected in HI by van Gorkom et al. (1989). However, it seems a much more extreme object, having also been singled out as an ultra-luminous infrared galaxy (ULIRG) by Sanders et al. (1988), with an IRAS luminosity of  $10^{12.44} L_\odot$ . The host galaxy of PKS 1345+12 has an irregular optical morphology, with two nuclei separated by  $3.0''$  and prominent tidal tails; thus it is almost certainly a merger event in progress. In addition, in PKS1345+12 we also see large amounts of nuclear obscuration, and CO (Evans et al. 1999) and OH megamaser (Baan, Salzer & Lewinter 1998) emission centered on the western nucleus, which is also the location of the AGN. Evans et al. (1999) attempt to link the molecular gas with the feeding and development of the AGN. Hurt et al. (1999) reported a UV

polarization of  $16.4 \pm 2.6\%$  in HST/FOC observations, with a polarization PA nearly perpendicular to the radio axis, consistent with scattered AGN light. However there is inadequate astrometric information to associate the polarized UV source with the AGN. The X-ray data are consistent with a hard power-law spectrum plus a large ( $> 10^{22} \text{ cm}^{-2}$ ) absorbing column (O’Dea et al. 1996b, Imanishi & Ueno 1999)

Nine  $z > 0.2$  CSOs have been observed with HST (DeVries et al. 2000, Perlman et al. 2001, McHardy et al. 1994). All of the DeVries et al. objects are well fit by elliptical models, and none show irregular isophotes (although n.b., De Vries et al. do not discuss variations in PA or ellipticity) or strong obscuration features, although three are significantly reddened: 0404+768 ( $z = 0.599$ ), 0428+205 ( $z = 0.219$ ) and 0500+019 ( $z = 0.583$ ), all of which also have close companions. But due to their much greater distances, the lack of (e.g.) visible dust features and/or aligned structures in the remaining sources cannot be taken as a statement that they do not exist. In fact, only for the very nearest of the three reddened sources in the DeVries et al. sample (0428+205) could HST resolve features similar in size to those observed in the nuclear regions of these three objects. Moreover, the DeVries et al. observations were carried out in redder bands (NICMOS F110W and F205W) so that their sensitivity to modest amounts of dust was much less. PKS 1413+135, analyzed by Perlman et al. (in prep.) and McHardy et al. (1994), appears to be a very different object, having a clearly spiral host, but strong nuclear and galaxy wide obscuration, molecular absorption (Wiklind & Combes 1994, 1997), and a hard, obscured X-ray source (Sugihara et al. 1999); the latter properties being similar to PKS 1345+12.

In summary, the three CSOs imaged here appear to be relatively normal, albeit relatively dusty luminous elliptical galaxies. They also appear to be representative of the CSO class, although a few CSOs (e.g., PKS 1345+12 and PKS 1413+135) appear to be more obvious candidates for very recent merger events.

Since mergers tend to force gas and dust towards the central regions (Mihos & Hernquist 1996), the large dust masses of 1146+596, 4C 31.04 and 1946+708, are interesting in the light of the scenario proposed by Wilson & Colbert (1995), whereby the “turn-on” of nuclear activity is triggered by a merger event. Also interesting is the presence of companions within 20-70 kpc projected distance, for all three objects. But perhaps most interesting of all in this light is that these objects appear to have outwardly normal isophotal profiles (fitting nuker models rather well), but exhibit significant anomalies in PA and ellipticity, particularly in their inner regions. This is consistent with the finding of Mihos (1995) that  $\gtrsim 10^8$  years after a major merger of two disk galaxies, the inner 3-5 kpc region of the remaining galaxy appears quite similar to a normal elliptical in its surface brightness profile but with remnant ellipticity changes and isophotal twists. Thus if a major merger triggered the activity seen in these objects, it must have occurred  $\gtrsim 10^8$  years earlier (cf. Mihos 1995, Hernquist & Mihos 1995, Mihos & Hernquist 1996).

A timescale of  $> 10^8$  years after a major merger is similar to the timescale over which a  $10^8 M_\odot$  black hole could double its mass while accreting at the Eddington rate (the Eddington rate

is  $\sim 3 M_{\odot} \text{ yr}^{-1}$  for a  $10^8 M_{\odot}$  black hole, and scales linearly with the mass), and is also of the same order as the timescale required to accrete material into the inner few parsecs of a galaxy ( i.e., the dynamical time of the “nested bars” hypothesis of Shlosman et al. 1989). These timescales are relevant if indeed the “activation” of a radio-loud AGN is directly related to spinning up of the nuclear black hole (see, e.g., Meier 1999, Reynolds et al. 1999); a significant increase in the black hole’s angular momentum would require the accretion of a mass comparable to the mass of the black hole. This long time delay between the merger and the onset of nuclear activity could also be due to the long time required for a bound black hole binary to coalesce (or for a hard black hole binary to form - see Begelman et al. 1980), although recent simulations indicate that the coalescence timescale for black hole binaries is almost certainly much longer than  $10^8$  years (Merritt, Cruz & Milosavljevic 2000; Poon & Merritt 2001), as required by the Wilson & Colbert (1995) scenario. In either case, our observations require that if a major merger is responsible for the onset of nuclear activity, a mechanism with timescale  $\sim 10^8$  years must delay the production of the radio source. Simulations of mergers (Mihos & Hernquist 1996) suggest that gas inflow into the nuclear regions of the product galaxy would peak  $\sim 5 - 10 \times 10^7$  years after the beginning of the merger, and continue for several  $\times 10^7$  years.

A timescale of  $\sim 10^8$  years is also important to our understanding of these objects for another reason: by the time that long of a time period has elapsed, any nuclear starburst associated with the merger will have subsided, although some evidence may remain in the colors. We do not see any evidence of nuclear starbursts in these objects, with the possible exception of the near-IR “bar” in 1146+596. De Vries et al. (1998a, 1998b, 2000) also found that the colors of CSO host galaxies at higher redshifts were consistent with predominantly old stellar populations.

Our findings are also consistent with more quiescent feeding mechanisms for a pre-existing black hole. For example, a more distant tidal encounter could alter the gravitational potential of the inner few kpc of these galaxies, driving gas radially inward as in the “nested bars” hypothesis of Shlosman et al. (1989). Our discovery of a stellar bar in the nearest of these objects is surprising and constitutes strong support for the “nested bars” hypothesis. The presence of more distant ( $20 - 70 h_{60}^{-1}$  kpc) companions in all three cases is also important in this regard. Tidal encounters with these companions could also produce the isophotal anomalies we observe, and would also be consistent with a less-violent mode for nuclear star formation, thus lessening the effect of a nuclear superwind on the fuelling of the nascent central engine. If indeed tidal encounters or other more quiescent methods are the preferred way to trigger nuclear activity in AGN, these objects may not be in their first active phase. In this case, we might expect to find evidence for previous nuclear activity due to previous tidal encounters with companion galaxies. By contrast, in the merger scenario, relic haloes are much harder to explain and would not be expected.

Previous authors (e.g., Conway 1996 and sources therein) have cited the kpc-scale radio halo of 1146+596 as evidence of a possible previous active stage, perhaps indicative of a recurrent radio source (e.g., Reynolds et al. 1997). Similar statements have been made for 3C 236 (O’Dea et al. 2001, Schilizzi et al. 2001), a CSS with both compact, 2 kpc-size inner radio lobes and a Mpc-scale

radio halo. The size of the variations in isophotal PA and ellipticity seen in 3C 236 are similar to those we see in 1146+596, as are the mass and relative orientation of its nuclear dust disk, and the amount of larger-scale dust features. 3C 236 also has evidence for recent star formation of varying ages in these dust features. O’Dea et al. (2001) suggest on the basis of these features that the fuel supply to the AGN in 3C 236 was interrupted for  $\sim 10^7$  years and is now restored. They argue in favor of a non-steady transport of gas in the disk and more quiescent triggering of active stages based on gas-dynamical processes.

In the light of these findings, further observations of nearby CSOs are warranted. The results of a sensitive 90 cm VLA search for very steep spectrum, aged radio remnants around CSOs would be an important discriminant between the merger and more quiescent triggering scenarios. Emission-line imaging and spectra of these objects with HST would allow us to disentangle their nuclear kinematics and dynamics, enabling us to relate the dust, gas disks and any nuclear star formation to the feeding and triggering of the nuclear activity. Finally, observations of many more nearby CSOs (including objects *not* selected for large obscuring columns) are needed to substantiate the results from this very small sample, and hopefully give us more concrete evidence regarding the Wilson & Colbert (1995) scenario that radio galaxy activity is triggered by major merger events.

We wish to thank Al Schultz, Howard Bushouse and Eddie Bergeron for considerable help with the HST data reductions. We also wish to thank an anonymous referee for many suggestions which significantly improved this paper. We thank Peter Barthel, Eleni Chatzichristou, Tim Heckman, Susan Neff, Chris O’Dea, Alison Peck, Eric Smith and Greg Taylor for interesting discussions. Support for proposal GO-7344 was provided by NASA through a grant from the Space Telescope Science Institute, which is operated by the Association of Universities for Research in Astronomy, Inc., under NASA contract NAS5-26555. ESP acknowledges support at Johns Hopkins University and the University of Maryland from NASA LTSA grant NAG5-9534/NAG5-9997 and HST grant GO-8060. CR acknowledges support at the University of Colorado from Hubble Fellowship HF-01113.01-98A.

## REFERENCES

- Baan, W. A., Salzer, J. J., & Lewinter, R. D., 1998, *ApJ*, 509, 633.
- Begelman, M. C., Blandford, R. D., & Rees, M. J., 1980, *Nature*, 287, 307.
- Bender, R., 1988, *A & A*, 193, L7
- Bender, R., Döbereiner, S., & Möllenhoff, C., 1988, *A & A S*, 74, 385.
- Bohlin, R. C., Savage, B. D., & Drake, J. F., 1978, *ApJ*, 224, 132.
- Byun, Y.-I., Grillmair, C. J., Faber, S. M., Ajhar, E. A., Dressler, A., Kormendy, J., Lauer, T. R., Richstone, D., Tremaine, S., 1996, *AJ*, 111, 1889.
- Carilli, C. L., Perlman, E. S., & Stocke, J. T., 1992, *ApJL*, 400, L13.
- Chiaberge, M., Capetti, A., & Celotti, A., 1999, *A & A*, 349, 77.
- Conway, J. E. 1996, *The Second Workshop on Gigahertz Peaked Spectrum and Compact Steep Spectrum Radio Sources*, ed. I. A. G. Snellen, R. T. Schilizzi, H. J. A. Röttgering, and M. N. Bremer, p. 198.
- Conway, J. E., 1999, *NAR*, 43, 509.
- Conway, J. E., 2000, in *Lifecycles of Radio Galaxies*, ed. J. Biretta, A. Koekemoer, C. O’Dea & E. Perlman, *NAR*, in press.
- Conway, J. E., 2001, *IAU Symposium 205*, ‘Galaxies and their contents at the highest resolution’, in press.
- De Koff, S., et al. 2000, *ApJS*, 129, 33.
- De Vaucouleurs, G., 1976, “Second Reference Catalogue of Bright Galaxies” (Austin: University of Texas Press).
- De Vaucouleurs, G., 1991, “Third Reference Catalogue of Bright Galaxies” (New York: Springer-Verlag).
- De Vries, W., et al. 1998a, *ApJ*, 503, 138.
- De Vries, W., et al. 1998b, *ApJ*, 503, 156.
- De Vries, W., O’Dea, C., Barthel, P., Fanti, C., Fanti, L., & Lehnert, M. D., 2000, *AJ*, 120, 2300.
- Dickey, J., 1986, *ApJ*, 300, 190.
- Evans, A. S., Kim, D. C., Mazzarella, J. M., Scoville, N. Z., & Sanders, D. B., 1999, *ApJ*, 521, L107.
- Faber, S. M., et al. 1997, *AJ* 114, 1771.
- Fanti, R., Fanti, C., Schilizzi, R., Spencer, R., Redong, N., Parma, P., Van Breugel, W., & Venturi, T., 1990, *A & A*, 231, 333.
- Forbes, D. A., 1991, *MNRAS*, 249, 779.



- Fosbury, R. A. L., Bird, M. C., Nicholson, W., & Wall, J. V., 1987, MNRAS, 225, 761.
- van Gorkom, J. H., Knapp, G. R., Ekers, R. D., Ekers, D. D., Laing, R. A., & Polk, K. S., 1989, AJ, 97, 708.
- Goudfrooij, P., De Jong, T., Hansen, L., Norgaard-Nielsen, H. U., 1994a, MNRAS, 271, 833.
- Goudfrooij, P., Hansen, L., Jorgensen, H. E., & Norgaard-Nielsen, H. U., 1994b, A & A S, 105, 341.
- Hernquist, L., & Mihos, J. C., 1995, ApJ 448, 41.
- Hurt, T., Antonucci, R., Cohen, R., Kinney, A., & Krolik, J., 1999, ApJ, 514, 579.
- Imanishi, M., & Ueno, S., 1999, ApJ, 527, 709.
- Impey, C. D., Wynn-Williams, C. G., Becklin, E. E., 1990, ApJ, 356, 621.
- Kim, D.-W., 1989, ApJ, 346, 653.
- Ledlow, M. J., & Owen, F. N., 1995, AJ, 110, 1959.
- Lin, H., Kirshner, R. P., Shectman, S. A., Landy, S. D., Oemler, A., Tucker, D. L., & Schechter, P. L., 1996, ApJ, 464, 60.
- Martel, A. R., et al., 1999, ApJ, 122, 81.
- Martel, A. R., et al., 2000, ApJ, in press.
- Mathis, J. S., 1990, ARAA, 28, 37.
- McHardy, I. M., Merrifield, M. R., Abraham, R. G., & Crawford, C. S., 1994, MNRAS, 268, 681.
- Meier, D. L., 1999 ApJ, 522, 753.
- Merritt, D., Cruz, F., Milosavljevic, M., 2000, in “Dynamics of Star Clusters”, ed. S. Deiters et al., in press, astro-ph/0008497.
- Mihos, J. C., 1995, ApJL, 438, L75.
- Mihos, J. C., & Hernquist, L., 1996, ApJ, 464, 641.
- Mihos, J. C., Walker, I. R., Hernquist, L., Mendes de Oliveira, C., & Bolte, M., 1995, ApJ 447, L87.
- Murgia, M., Fanti, C., Fanti, R., Gregorini, L., Klein, U., Mack, K. – H., & Vigotti, M., 1999, A & A, 345, 769.
- NICMOS team, “NICMOS Photometry Update,” 1999, <http://www.stsci.edu/cgi-bin/nicmos>
- Nieto, J. L., & Bender, R., 1989, A & A, 215, 266.
- Nieto, J. L., Poulain, P., & Davoust, E., 1994, A & A, 283, 1.
- Nilson, P., 1973, “Uppsala General Catalogue of Galaxies,” Nova Acta Regiae Soc. Sci. Upsaliensis, Ser. V:A, 1.
- O’Dea, C. P., 1998, PASP, 110, 493.

- O’Dea, C. P., Koekemoer, A. M., Baum, S. A., Sparks, W. B., Martel, A. R., Allen, M. G., Macchetto, F. D., & Miley, G. K., 2001, *AJ*, in press (astro-ph/0101441).
- O’Dea, C. P., Stanghellini, C., Baum, S. A., & Charlot, S., 1996a, *ApJ*, 470, 806.
- O’Dea, C. P., Worrall, D. M., Baum, S. A., & Stanghellini, 1996b, *AJ*, 111, 92.
- Owen, F. N., & Laing, R. A., 1989, *MNRAS*, 238, 357.
- Owsianik, I., & Conway, J. E., 1998, *A & A*, 337, 69.
- Owsianik, I., Conway, J. E., & Polatidis, A. G., 1998, *A & A*, 336, 37.
- Peck, A. B., & Taylor, G. B., 1998, *ApJ*, 502, L23.
- Peck, A. B., Taylor, G. B., & Conway, J. E., 1999, *ApJ*, 521, 103.
- Perlman, E. S., Carilli, C. L., Stocke, J. T., & Conway, J. E., 1996, *AJ*, 111, 1839.
- Perlman, E. S., Stocke, J. T., Shaffer, D. B., Carilli, C. L., & Ma, C., 1994, *ApJL*, 424, L69.
- Perlman, E. S., Stocke, J. T., Carilli, C. L., & Conway, J. E., Wang, Q. D., Tashiro, M., & Sugihro, M., 2001, in preparation
- Poon, M. Y., Merritt, D., 2001, *ApJ*, 549, 192.
- Readhead, A. C. S., Xu, W., Pearson, T. J., Wilkinson, P. N., & Polatidis, A. G., 1994, in *Compact Extragalactic Radio Sources (1994 NRAO Symposium)*, eds. Zensus, A., & Kellerman, K., (ASP: Provo), pp. 17-22.
- Readhead, A. C. S., Taylor, G. B., Xu, W., Pearson, T. J., Wilkinson, P. N., & Polatidis, A. G., 1996a, *ApJ*, 460, 612.
- Readhead, A. C. S., Taylor, G. B., Pearson, T. J., & Wilkinson, P. N., 1996b, *ApJ*, 460, 634.
- Rest, A., van den Boesch, F. C., Jaffe, W., Tran, H., Tsvetanov, Z., Ford, H. C., Davies, J., & Schafer, J., 2001, *AJ*, in press, astro-ph/0102286.
- Reynolds, C. S. & Begelman, M. C., 1997, *ApJ*, 488, 109.
- Reynolds, C. S., Young, A. J., Begelman, M. C., & Fabian, A. C., 1999, *ApJ*, 514, 164.
- Sandage, A., & Tamman, G. A., 1981, “A Revised Shapley-Ames Catalog of Bright Galaxies” (Washington: Carnegie Institution).
- Sanders, D. B., Soifer, B. T., Elias, J. H., Neugebauer, G., & Matthews, K. 1988, *ApJ*, 328, L35.
- Scarpa, R., Urry, C. M., Falomo, R., Pesce, J. E., Webster, R., O’Dowd, M., & Treves, A., 1999, *ApJ*, 521, 134.
- Scarpa, R., Urry, C. M., Falomo, R., Pesce, J. E., Treves, A., 2000, *ApJ*, 532, 740.
- Schilizzi, R. T., Tian, W. W., Conway, J. E., Nan, R., Miley, G. K., Barthel, P. D., Normandean, M., Dallacasa, D., and Gurvits, L. I., 2001, *A & A*, 368, 398/.
- Scoville, N. Z., Evans, A. S., Thompson, R., Rieke, M., Hines, D. C., Low, F. J., Dinshaw, N., Surace, J. A., & Armus, L., 2000, *AJ*, 119, 991.

- Shlosman, I., Frank, J., & Begelman, M. C., 1989, *Nature*, 338, 45.
- Smith, E. P., & Heckman, T. M., 1989, *ApJS* 69, 365.
- Snellen, I. A. G., Bremer, M. N., Schilizzi, R. T., Miley, G. K. & Van Oje, R., 1996, *MNRAS*, 279, 1294.
- Snellen, I. A. G., et al. 1998, *MNRAS*, 301, 985.
- Stocke, J. T., Wurtz, R., Wang, Q., Elston, R., & Jannuzi, B., 1992, *ApJL*, 400, L17.
- Sugiho, M., Tashiro, M., Perlman, E. S., Makashima, K., Stocke, J. T., Wang, Q. D., & Madejski, G., 1999, *Astronomische Nachrichten*, 320, 316.
- Surace, J. A., Sanders, D. B., Vacca, W. D., Veilleux, S., & Mazzarella, J. M., 1998, *ApJ*, 492, 116.
- Taylor, G. B., Readhead, A. C. S., & Pearson, T. J., 1996, *ApJ*, 463, 95.
- Taylor, G. B., & Vermeulen, R. C., 1997, *ApJ*, 485, L9.
- Taylor, G. B., Wrobel, J. M., & Vermeulen, R. C., 1998, *ApJ*, 498, 619.
- Tran, H. D., Tsvetanov, Z., Ford, H. C., Davies, J., Jaffe, W., van den Bosch, F. C., & Rest, A., 2001, *AJ*, in press, astro-ph/0102292.
- Urry, C. M., Scarpa, R., O’Dowd, M., Falomo, R., Pesce, J. E., & Treves, A., 2000, *ApJ*, 532, 816.
- van der Marel, R., 1998, <http://sol.stsci.edu/marel/software/pedestal.html>
- Wiklind, T., & Combes, F., 1994, *A&A*, 286, L9.
- Wiklind, T., & Combes, F., 1997, *A & A*, 328, 48.
- Wilson, A. S., & Colbert, E. J. M., 1995, *ApJ*, 438, 62.

Left empty because of its size. Figure included as JPG

Left empty because of its size. Figure included as JPG

Left empty because of its size. Figure included as JPG

Left empty because of its size. Figure included as JPG

Fig. 4.— Host Galaxy surface brightness profiles of all three objects. At left, 1146+596, center, 4C31.04, and at right, 1946+708. All error bars plotted here are  $1\sigma$ . The dotted line in the top panels represents the best fit “nuker” model (see Table 2 and §3.2 for details). In the cases of 4C 31.04 and 1946+708 we have excluded regions where the parameter fits did not converge or gave

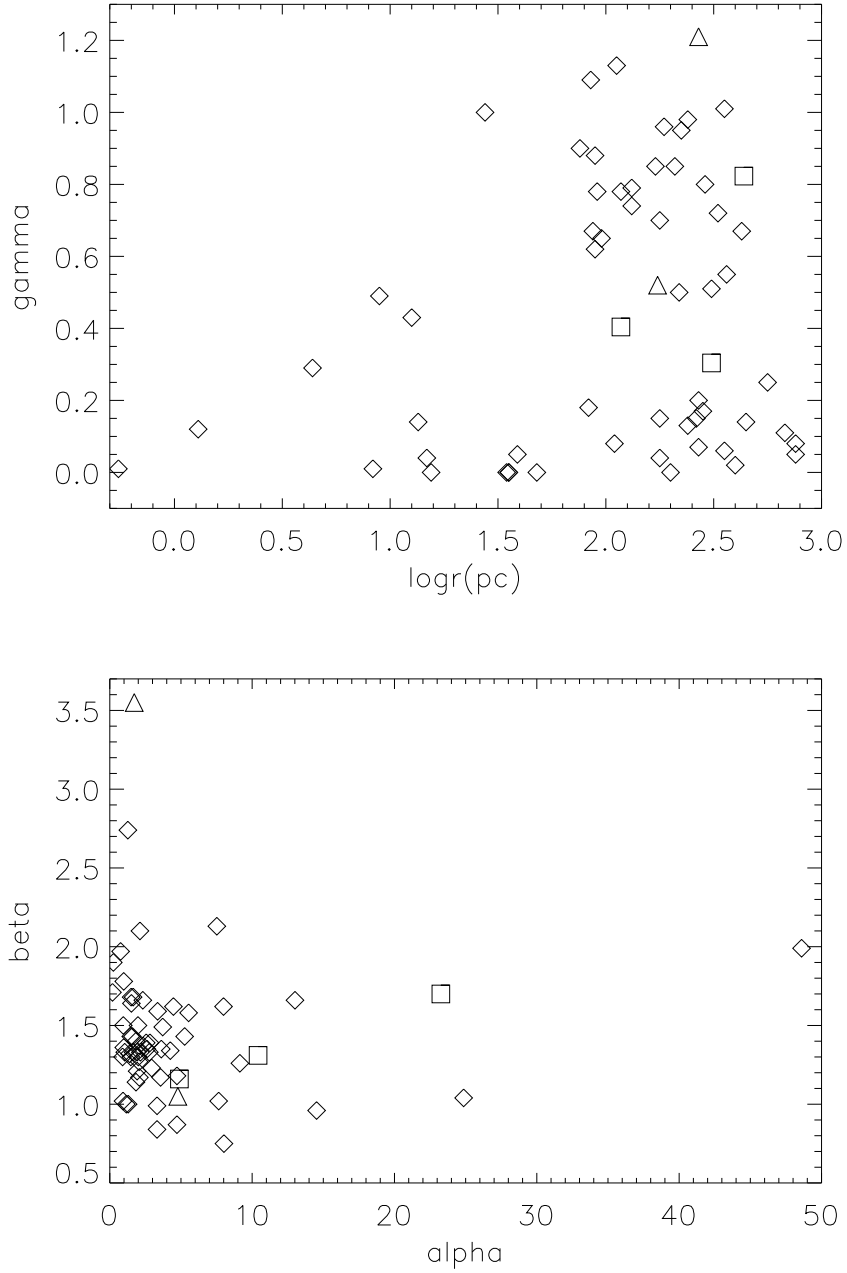


Fig. 5.— Nuker fit parameters for these three objects, compared to the objects in the Faber et al. (1997) sample. Our objects are the squares in this plots, and the Faber et al. objects are the diamonds, while the triangles are Faber et al.’s simulations of M31 and M32 (respectively) at the distance of the Virgo cluster. While these objects appear to be rather intermediate between the “core” and “power-law” galaxy types, this is likely a product of their several times greater distance compared to the objects in the Faber et al. sample. See §4 for discussion.



Left empty because of its size. Figure included as JPG

This figure "Perlman\_fig1.gif" is available in "gif" format from:

<http://arxiv.org/ps/astro-ph/0104439v2>

This figure "Perlman\_fig2.gif" is available in "gif" format from:

<http://arxiv.org/ps/astro-ph/0104439v2>

This figure "Perlman\_fig3.gif" is available in "gif" format from:

<http://arxiv.org/ps/astro-ph/0104439v2>

This figure "Perlman\_fig4.gif" is available in "gif" format from:

<http://arxiv.org/ps/astro-ph/0104439v2>

This figure "Perlman\_fig6.gif" is available in "gif" format from:

<http://arxiv.org/ps/astro-ph/0104439v2>

Table 1. Log of HST Observations

Object	Instrument	Filter	Date	Exposure (s)	RA (J2000)	Dec
4C31.04	NICMOS	F160W	Dec 17 1997	2560	01 19 35.05	+32 10 50.27
4C31.04	WFPC2	F450W	Nov 24 1998	1600	01 19 32.37	+32 10 50.17
4C31.04	WFPC2	F702W	Nov 24 1998	520	01 19 32.37	+32 10 50.17
1146+596	NICMOS	F160W	Aug 3 1997	2816	11 48 50.34	+59 24 55.93
1146+596	WFPC2	F450W	Dec 2 1998	1600	11 48 54.01	+59 24 44.14
1146+596	WFPC2	F702W	Dec 2 1998	600	11 48 54.01	+59 24 44.14
1946+708	NICMOS	F160W	Aug 17 1997	2816	19 45 53.57	+70 55 48.85
1946+708	WFPC2	F450W	Aug 31 1998	1600	19 45 50.01	+70 56 04.36
1946+708	WFPC2	F702W	Aug 31 1998	700	19 45 50.01	+70 56 04.36

Table 2. Basic Data - CSO Host Galaxies

Object	$z$	$h_{60}^{-1} \text{pc}''$	$r_b$ (pc)	$\alpha$	$\beta$	$\gamma$	$M_H$	$\langle B - R \rangle$	$\langle R - H \rangle$
1146+59	0.0107	216	$933 \pm 1$	$4.89 \pm 0.15$	$1.169 \pm 0.001$	$0.404 \pm 0.006$	-21.80	$1.60 \pm 0.08$	$0.90 \pm 0.05$
4C 31.04	0.057	1014	$308 \pm 2$	$10.42 \pm 0.90$	$1.314 \pm 0.002$	$0.295 \pm 0.011$	-23.59	$1.68 \pm 0.18$	$1.30 \pm 0.09$
1946+708	0.101	1687	$437 \pm 5$	$23 \pm 10$	$1.699 \pm 0.004$	$0.823 \pm 0.030$	-23.77	$1.56 \pm 0.61$	$1.25 \pm 0.21$

Table 3. Absorption Data - CSO Host Galaxies

Object	Feature	$A_B^1$	$N_H^1 (10^{20} \text{ cm}^{-2})$	$T_s/f_c$ (K)	$M_H^1 (10^5 M_\odot)$
1146+59	Average/Total	0.30 (avg)	4.3 (avg)	...	2.5 (tot)
	NW mini-jet	0.86	13	100	
	SE mini-jet	0.87	13	78	
4C 31.04	Average/Total	0.46 (avg)	6.6 (avg)	...	4.8 (tot)
	E mini-lobe	1.92	28	150	
	W mini-lobe	1.05	15	220	
1946+708	Average/Total	0.70	10	...	7.3 (tot)
	NE mini-lobe	1.61	23	160	
	SW mini-lobe	0.74	11	70	

<sup>1</sup>See text for explanation of procedure